

RESEARCH

Open Access



Emerging zoonotic potential of H4N1 avian influenza virus: enhanced human receptor binding and replication via novel mutations

Xiaobin Peng^{1*}, Xianxian Wen¹, Jing Deng¹, Mengyuan Yuan¹, Yang Liu¹, Yunqiu Zhou¹, XuBin Du¹, Han Yang¹, Guangqun Jiang¹, Xumei Li², Feng Yin², Ping Liu³, Yun Tang⁴, Zhangping Tan⁴, Zhen Yu⁴ and Shuang Chen^{4*}

Abstract

Background Avian influenza virus (AIV), a zoonotic pathogen found worldwide, includes multiple subtypes, one of which is the H4 subtype frequently detected in wild birds and poultry. Despite its prevalence, research on H4 subtype AIV has been scarce, with a focus predominantly on the H4N2 and H4N6 subtypes. The zoonotic potential of H4N1 has not been investigated to date.

Methods In this study, we used gene sequencing in conjunction with bioinformatics methodologies to analyze wild-type H4N1 AIV strain and mutant strains emerging from serial passaging in cell culture. Furthermore, we assessed the zoonotic potential of H4N1 and the alterations caused by mutations via a series of phenotype assays, including evaluation of receptor binding affinity, immunofluorescence assays, analyses of growth kinetics across different animal cell cultures, and in vivo pathogenicity studies.

Results Our research reveals that H4N1 AIV can bind to human receptors and exhibits an affinity for human lung and tracheal tissues. In vitro experiments demonstrate that H4N1 replicates efficiently in human cell lines. Furthermore, animal studies demonstrate that H4N1 can induce pneumonia in mice without the need for prior adaptation to the host. Notably, during passage in cell culture, H4N1 rapidly acquired two previously unreported mutations. These mutations significantly enhanced the virus's ability to attach to human receptors and its capacity for replication.

Conclusions In summary, our study provides preliminary experimental evidence for the emerging zoonotic potential of H4N1 AIV. These findings expand our knowledge of the H4 subtype AIV and reinforce the critical need for continued surveillance of AIV to prevent and prepare for potential outbreaks affecting human health.

Keywords Avian influenza virus, Novel H4N1 subtype, Zoonotic potential, Public health, One health

*Correspondence:

Xiaobin Peng
pengxiaobin85@163.com
Shuang Chen
39690490@qq.com

¹Chongqing Changshou Center for Disease Control and Prevention, Chongqing, China

²Department of Pathology, Chongqing Changshou District Maternal and Child Health Hospital, Chongqing, China

³Department of Respiratory and Critical Care Medicine, The People's Hospital of Changshou District, Chongqing, China

⁴Chongqing Center for Disease Control and Prevention, Chongqing, China



© The Author(s) 2025. **Open Access** This article is licensed under a Creative Commons Attribution-NonCommercial-NoDerivatives 4.0 International License, which permits any non-commercial use, sharing, distribution and reproduction in any medium or format, as long as you give appropriate credit to the original author(s) and the source, provide a link to the Creative Commons licence, and indicate if you modified the licensed material. You do not have permission under this licence to share adapted material derived from this article or parts of it. The images or other third party material in this article are included in the article's Creative Commons licence, unless indicated otherwise in a credit line to the material. If material is not included in the article's Creative Commons licence and your intended use is not permitted by statutory regulation or exceeds the permitted use, you will need to obtain permission directly from the copyright holder. To view a copy of this licence, visit <http://creativecommons.org/licenses/by-nc-nd/4.0/>.

Introduction

Influenza A virus (IAV) is a significant global public health threat. As a zoonotic pathogen, IAV can infect a wide range of species, some of which cause infection in humans [1]. Based on the differences in two surface glycoproteins: hemagglutinin (HA) and neuraminidase (NA), IAVs can be classified into multiple subtypes [2]. Among them, avian influenza viruses (AIVs) from waterfowl have 16 HA subtypes (H1-H16) and 9 NA subtypes (N1-N9) [3], whereas IAV-like viruses from bats have 2 subtypes (H17N10 and H18N11) [4]. Some researchers suggest that influenza viruses in poultry and mammals, including humans, have evolved either directly or indirectly from AIVs [5]. Occasionally, AIVs spilled over into the human population, resulting in sporadic infections and occasional epidemics [6]. For instance, AIV subtypes H5, H6, H7, H9, and H10 have been responsible for tens of thousands of infections and thousands of fatalities globally [7]. Notably, the H5N1 AIV clade 2.3.4.4b is currently circulating across several states in the United States and has spilled over to multiple species, including humans, with the potential to trigger a new outbreak [8]. This development has drawn considerable attention from the virology community. The possibility that other subtypes, such as the H4 subtype commonly detected in wild birds and poultry [9, 10], may also pose a risk of spillover remains an open question.

Since its initial isolation from a duck in 1956, the H4 subtype has been documented across a wide range of hosts, including various avian species [11–14], as well as mammals [15, 16]. These findings suggest that the H4 subtype AIV possesses the capability to cross species barriers and is capable of infecting mammals. Nevertheless, research on the H4 subtype AIV remains limited, particularly regarding its zoonotic potential, with the majority of studies concentrating on specific subtypes such as H4N2 and H4N6 [17, 18]. Consequently, there is a pressing need for further data to deepen our insights into this specific AIV subtype.

To deepen our understanding of the H4 subtype AIV, we performed an extensive detection of a novel and rare H4N1 AIV to assess its zoonotic potential. Our objectives focus on characterizing the profile of H4N1 AIV isolated from live poultry market environments, identifying adaptive mutations that emerged from serial passaging in cell culture, and assessing the functional implications of these mutations for zoonotic potential via human receptor binding assays, replication kinetics, and murine pathogenicity studies.

Materials and methods

Ethical statements

All experiments involving non inactivated samples, except for animal experiments, were performed in the

biosafety level 2 facility at the Changshou Center for Disease Control and Prevention, in strict accordance with the recommendations of the institutional biosafety manual. Animal experiments were carried out at Charles River Laboratories and were approved by the Institutional Animal Care and Use Committee (IACUC) of Charles River Laboratories (Permission number: BJ-GE-24-139), and all procedures complied with the welfare standards for laboratory animals.

Cell

Madin-Darby Canine Kidney (MDCK), human type II alveolar epithelial (A549), and chicken-origin fibroblast (DF-1) cells were purchased from Procell Life Technology Co., Ltd (www.procell.com.cn). All cell lines were subjected to short tandem repeat (STR) profiling to ensure no misidentification or cross-contamination and were cultured according to the manufacturer's recommendations.

Viruses

The virus A/environment/chongqing/cs2301/2022 (abbreviated as CS01) is multiple reassortant strain isolated from environmental samples collected in live poultry markets. A/A549/chongqing/cs2301-A4/2024 (abbreviated as CS01-A4) is a mutant strain derived from CS01 by continuous passage in A549 cells for 4 generations. A/A549/chongqing/cs2301-A7/2024 (abbreviated as CS01-A7) a mutant strain derived from CS01-A4, which was further passaged for 3 generations in A549 cells. The virus A/human/chongqing/F283/2024 (abbreviated as F283-H1N1) is a human H1N1 influenza virus isolate obtained from nasopharyngeal swabs of influenza patients. Additionally, the viruses A/duck/chongqing/EWL19006/2019 (abbreviated as E006-H9N2) is H9N2 AIV isolated from duck feces. All viruses were isolated, purified, and sequenced by our laboratory, and the information was uploaded to the GISAID database. The Isolate ID can be found in the Availability of Data. The viruses were cultured in MDCK cells, and the culture medium was filtered through a 0.22- μ m filter membrane to prepare a virus suspension. After sub packaging, they were stored at -80 °C. The 50% tissue culture infectious dose (TCID₅₀) of each virus in MDCK cells was determined using the Reed-Muench method. These five viruses underwent exclusivity testing via genetic sequencing to ensure that the results corresponded to the correct single type, thereby ruling out the presence of other influenza virus subtypes.

Genetic sequencing and bioinformatics analysis

The Respiratory Microorganisms Genome Amplification Kit (MGI Tech) and the MGIEasy Fast PCR-Free FS Library Preparation Kit (MGI Tech) were used to

construct the sequencing library. After library preparation, sequencing was performed on the next-generation sequencing platform MGISEQ-200 (MGI Tech). To acquire complete influenza virus gene sequences, the generated sequencing data were analyzed using the FluTrack V1.0 bioinformatics tool (MGI Tech) [for further details, please refer to Supplementary Material S1]. Bioinformatics analysis was performed on the obtained sequence. GeneQuest 7.1.1.44 (DNASTAR Lasergene) was used to analyze open reading frames (ORFs) and amino acid sequences. Sequence similarity analyses were performed using MegAlign 7.1.0 (DNASTAR Lasergene). HA subtype amino acid sequences were aligned using the HA Subtype Numbering Conversion tool (<http://www.bv-brc.org/app/HASubtypeNumberingConversion>). Amino acid sequences were aligned and analyzed using MEGA-X 10.2.3 (<http://www.megasoftware.net>). Analysis of variant site information was performed using the GISAID EpiFlu Flusurver tool (<http://platform.epicov.org/epi3/frontend#3f13c3>).

Detection of Sialic acid receptors on the surface of red blood cells

Flow cytometry was used to detect sialic acid receptors on the surface of red blood cells. Sambucus Nigra Agglutinin (SNA) preferentially binds to sialic acid on the α -2,6-glycan linkage and has a lower degree of binding to the α -2,3 linkage [19]. In contrast, Maackia Amurensis Lectin (MAL) has the opposite binding preference [20]. Red blood cells were diluted to a concentration of 1×10^{10} cells/ml with normal saline. A 50- μ L aliquot of the diluted red blood cells was mixed with 20 μ L of APC-conjugated SNA (2 μ g/ml) (Qiyuebio) and 20 μ L of FITC-conjugated MAL (3 μ g/ml) (Qiyuebio). The mixture was vortexed and incubated at room temperature in the dark for 25 min. Following incubation, 450 μ L of normal saline was added to the mixture, which was then analyzed on a flow cytometer (Wellgrowtec). Fluorescence detection was performed by setting gates with SSC-H and FSC-H to measure APC and FITC fluorescence.

Removal of α 2,3-sialic acid from red blood cells and hemagglutination assays

α -2,3-Sialidase (TaKaRa) was diluted to a concentration of 5 U/ml. 200 μ L of the enzyme were mixed with 200 μ L of guinea pig red blood cells, and the mixture was incubated at 37 °C for 30 min to remove α 2,3 sialic acid from the surface of the red blood cells. Following incubation, the treated red blood cells were washed three times with PBS to obtain a 1% red blood cell suspension. The suspension was prepared and used immediately to ensure experimental accuracy. The virus was diluted with normal saline to a titer of $1:2^6$ HA (using guinea pig red blood cells). 50 μ L of the diluted virus were then applied

to a 96-well cell culture plate with a U-shaped bottom for serial dilution. Then, 50 μ L of red blood cells were added to each well, and the plate was incubated at room temperature for 1 h.

Solid-phase binding assay

The receptor binding specificity was analyzed using a solid-phase binding assay [21]. Briefly, biotinylated polysaccharides 3'-SLN-C3-PAA-biot and 6'-SLN-C3-PAA-biot (GlycoNZ) were diluted in PBS, and 50 μ L of each dilution was added to streptavidin-coated high-binding 96-well plates (Pierce). The plates were incubated at room temperature for 2 h. Following removal of the glycopolymer solution, the plates were blocked with 100 μ L of PBS containing 5% BSA for 1 h at room temperature. The wells were then washed with ice-cold PBS containing 0.1% Tween 20 (PBST). Virus, diluted to 64HA units, was added to the wells and incubated overnight at 4 °C. After washing with PBST, 10% formalin was added to inactivate NA protein activity and incubated for 30 min at room temperature. The wells were washed again with PBST before adding mouse polyclonal antibodies (targeting the virus to be tested, prepared in-house) and incubating at 4 °C for 4 h. Subsequent to PBST washing, horseradish peroxidase-conjugated goat anti-mouse IgG (Sino Biological) was added and incubated at room temperature for 1 h. After another PBST wash, the plates were developed with 100 μ L of TMB horseradish peroxidase colorimetric solution (Beyotime) at room temperature for 15 min. The reaction was stopped with 50 μ L of 1 M H₂SO₄, and the absorbance was measured at 450 nm using an ELISA reader. Data were visualized using GraphPad Prism 8 software.

Fluorescence staining of human lung and tracheal tissues

The immunofluorescence assay was performed as previously described [22], with some modifications. Briefly, paraffin sections of airway and lung tissues (Tissue Array) were deparaffinized and rehydrated. Antigen retrieval was performed, followed by blocking with PBS containing 5% normal goat serum (Biosharp) at room temperature (RT) for 30 min to minimize non-specific binding. The sections were then incubated with 64 hemagglutinin (HA) units of the virus overnight at 4 °C. After washing with cold PBS, the sections were fixed with 10% formalin at RT for 30 min to inactivate neuraminidase (NA) protein activity, followed by another wash with cold PBS. Subsequently, the sections were incubated with mouse polyclonal antibodies (targeting the virus to be tested, prepared in-house) at 4 °C for 4 h. After washing with cold PBS, the sections were treated with a goat anti-mouse secondary antibody (Invitrogen) conjugated to FITC and incubated at RT in the dark for 1 h. Following another wash with cold PBS, the sections were stained

with DAPI dye (Invitrogen) for 10 min and then observed under a fluorescence microscope (Olympus). Fluorescent images were processed using ImageJ software.

Growth kinetics in different cell lines

To assess the *in vitro* growth kinetics of the virus, monolayers of MDCK, A549, and DF-1 cells were inoculated with the selected viruses at various multiplicity of infections (MOIs). The cells were first seeded onto a 6-well plate and allowed to reach approximately 90% confluence under optimal growth conditions. The growth medium containing serum was then removed, and the cells were washed with pre-warmed PBS. Subsequently, 200 μ L of the virus was added to each well and adsorbed at 37 °C for 1 h. Following adsorption, the virus solution was discarded, and the cells were overlaid with serum-free growth medium. The plates were then incubated at 37 °C in the presence of 5% CO₂. The supernatant was collected at 12, 24, 36, 48, 60, and 72 h post-inoculation. The viral titer in A549 and DF-1 cells was determined by TCID₅₀. For MDCK cells, the viral load was measured using a digital PCR instrument. Data were visualized using GraphPad Prism 8 software.

Experimental infections in mice

To assess the pathogenic potential of H4N1 AIVs in mammals, we inoculated BALB/c mice with CS01, CS01-A4, CS01-A7, and PBS (as a control). We monitored the changes in body weight of the mice over a 14-day period post-inoculation and determined the virus titers in various mouse organs. Six-week-old female BALB/c mice were acclimated for one week before being divided into groups. Three groups (9 mice per group) were intranasally inoculated with 50 μ L of CS01, CS01-A4, or CS01-A7 virus suspension, each containing 10⁶ TCID₅₀/100 μ L, to form the experimental groups. The virus solution was slowly and meticulously instilled into the nasal cavity of each mouse using a sterile pipette, ensuring that the process was gentle enough to prevent any risk of injury, without the need for anesthesia. Within each experimental group, we randomly divided the mice into a weight measurement subgroup (3 mice per group) and an anatomical subgroup (6 mice per group). Additionally, a control group was established, consisting of 3 mice inoculated with 50 μ L of PBS each. At 3 and 6 days post-inoculation (dpi), 3 mice from each anatomical subgroup were euthanized and dissected under sterile conditions to obtain tissue samples, including nasal turbinates, trachea, lungs, kidneys, and brain. Half of the tracheal and left lung tissues were fixed in 4% paraformaldehyde for histopathological sectioning, while the remaining tissues were precisely weighed and preserved at -80 °C for viral titer determination. For the determination of viral titer, the frozen tissue samples were thawed, and 1 mL of PBS

supplemented with ceramic beads was used to homogenize the tissues using a tissue homogenizer. Subsequently, the viral titer was determined by TCID₅₀ on MDCK cells. For the mice in the weight measurement subgroup, we monitored their body weight daily until the end of the 14-day observation period. These data were used to construct a weight change chart. Data were visualized using GraphPad Prism 8 software.

Results

Genetic sequencing and bioinformatics analysis

During growth kinetics assays, the CS01 H4N1 AIV was serially passaged in the cell line, resulting in the isolation of a series of mutated viruses. Notably, two mutant strains, CS01-A4 and CS01-A7, exhibited distinctive characteristics. These mutants showed higher virus yields and stronger cytotoxicity. Specifically, the viral load of these two mutant strains was more than fivefold higher than that of the wild-type CS01 at 36 h post-inoculation, and the onset of cellular pathology occurred more than 12 h earlier. Subsequent gene sequencing and amino acid sequence analysis revealed that, compared to CS01, the CS01-A4 and CS01-A7 mutants possess a R467Q substitution in the HA gene. Additionally, aside from the R467Q mutation, CS01-A7 also exhibits an A428T change in the NP gene. No substitutions were identified in other genes (Fig. 1). A detailed examination of these mutations indicates that the arginine residue (a polar basic amino acid) located at position 467 in the HA protein is replaced by glutamine (a polar neutral amino acid). Concurrently, the alanine residue (a non-polar amino acid) at position 428 in the NP protein is substituted with threonine (a polar neutral amino acid). Based on the analysis conducted using the EpiFlu Flusurver tool, both mutated residues are implicated in the viral oligomerization interfaces, and the R467Q mutation in the HA gene is associated with the binding of small ligands, indicating a potential role in modulating viral interactions with the host.

Hemagglutination assays

The specificity of the HA binding to α 2,6 sialic acid-linked polysaccharide receptors (human receptors) and to α 2,3 sialic acid-linked polysaccharide receptors (avian receptors) is acknowledged as a pivotal element in the transmission of influenza viruses, serving as the primary determinant of their host range [23]. To reveal this specificity, the hemagglutination assay is a classic method that utilizes red blood cells (RBCs) from different species or RBCs that have been treated with sialidase [24]. In this study, we performed hemagglutination assays using horse red blood cells (possess only α 2,3 sialic acid, abbreviated as α 2,3 RBCs) and sialidase-treated guinea pig red blood cells (possess only α 2,6 sialic acid, abbreviated as α 2,6

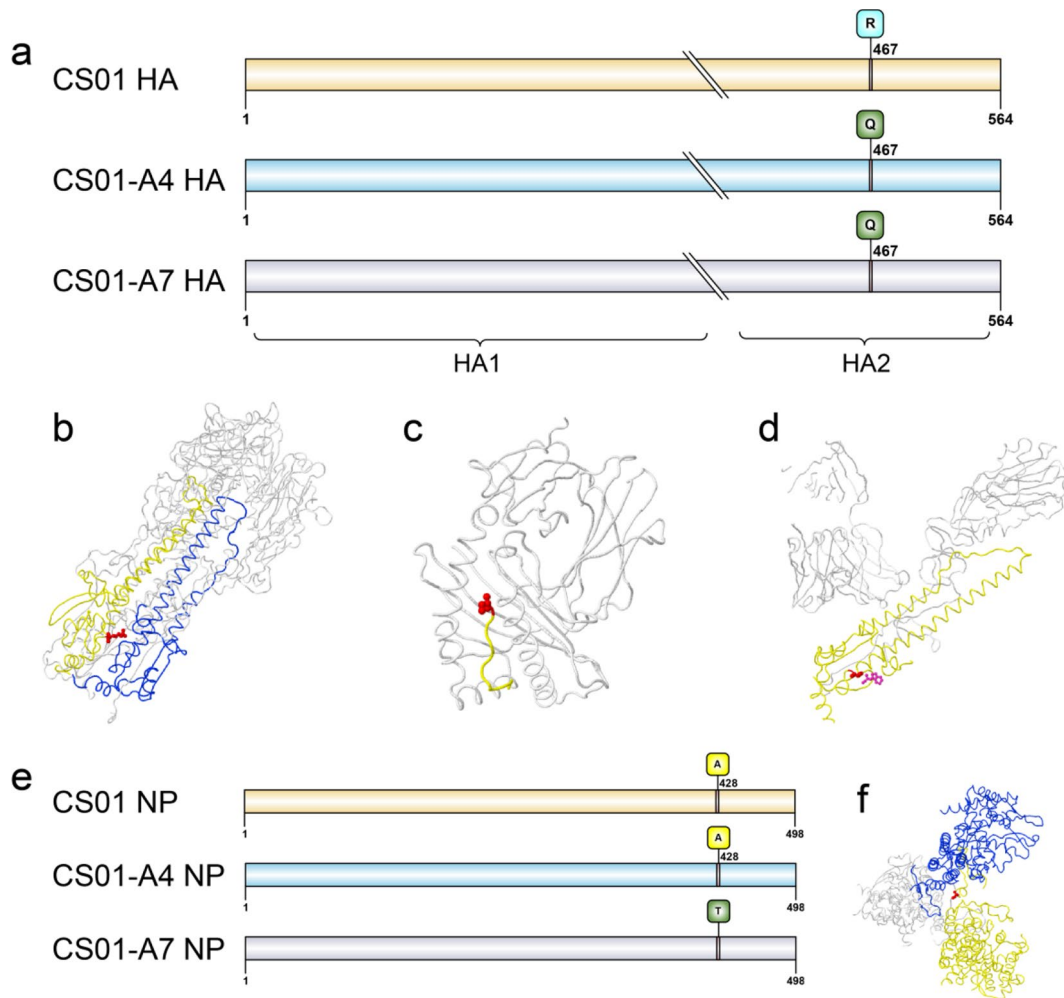


Fig. 1 The results of bioinformatics analysis for CS01, CS01-A4, and CS01-A7. **(a)** The positions of mutations in HA are compared among CS01, CS01-A4, and CS01-A7. **(b)** The R467Q mutation (indicated by red atoms) is located at position 124 on the viral chain F (with a yellow backbone) and is within a 5 Å distance from the oligomeric subunit chain D (with a blue backbone). **(c)** The R467Q mutation (red atoms) aligns with position 1 on the viral chain C (yellow backbone), and it is in close proximity, within 5 Å, to another structural element. **(d)** The R467Q mutation (red atoms) is also found at position 124 on the viral chain B (yellow backbone) and is within 5 Å of the ligand UNL (pink atoms). **(e)** The positions of mutations in NP are compared among CS01, CS01-A4, and CS01-A7. **(f)** The A428T mutation (red atoms) corresponds to position 428 on the viral chain A (yellow backbone) and is within a 5 Å range of the oligomeric subunit chain C (blue backbone)

RBCs) to assess the HA receptor-binding specificity of the H4N1 AIVs. The strains examined in this study comprised CS01, CS01-A4, CS01-A7, in addition to Human influenza virus F283-H1N1 and a AIV E006-H9N2 as control viruses. The results indicated that all three H4N1 AIVs possess the capacity to bind to RBCs with either α 2,3 sialic acid or α 2,6 sialic acid, while the human influenza virus F283-H1N1 only bind to α 2,6 sialic acid and AIV E006-H9N2 only bind to α 2,3 sialic acid (Fig. 2). These findings suggest that H4N1 AIVs can bind to both human and avian receptors simultaneously. Additionally, CS01-A4 and CS01-A7 demonstrated a higher affinity for human receptors compared to CS01.

Solid-phase binding assay

To further validate the receptor-binding specificity of the H4N1 AIVs, we used a solid-phase binding assay to reassess the binding capabilities of CS01, CS01-A4, and CS01-A7. This assay is an enhanced technique that allows for the direct quantification of a virus’s ability to bind to both α 2,3 and α 2,6 sialic acids (Fig. 3). The assay outcomes revealed that all three H4N1 AIVs were capable of binding to both α 2,3 and α 2,6 sialic acids, with a higher preference for α 2,3 sialic acids. Additionally, CS01-A4 and CS01-A7 demonstrated a greater binding capacity to α 2,6 sialic acids compared to CS01, aligning with the findings of the hemagglutination assay. These findings provide further evidence that H4N1 AIVs can simultaneously bind to both human and avian receptors, and

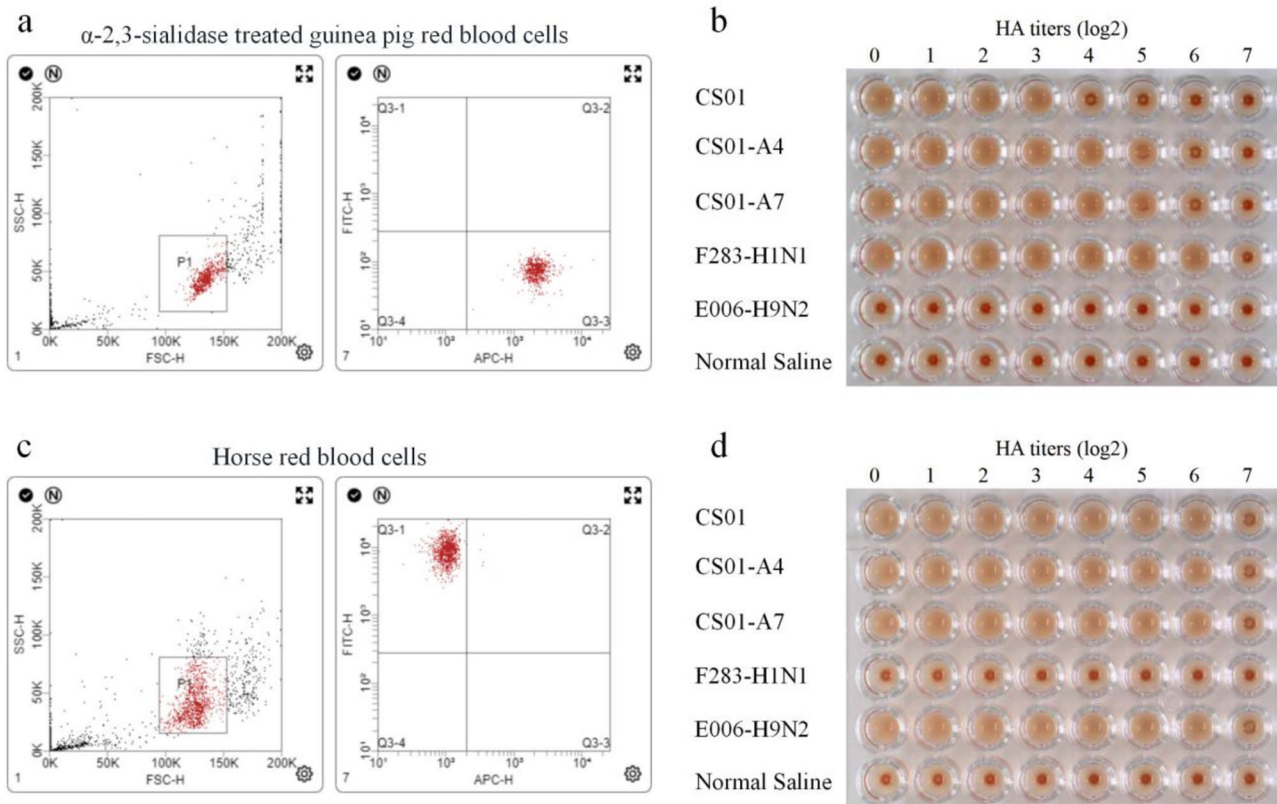


Fig. 2 Hemagglutination assay results for H4N1 AIVs. Flow cytometry analysis in (a) showed that the guinea pigs RBCs, treated with α 2,3 sialidase, were found to possess only α 2,6 sialic acid. (c) showed that horses RBCs contain exclusively α 2,3 sialic acid. The hemagglutination assay results using α 2,6 RBCs shown in (b), indicate that all three H4N1 AIVs are capable of binding to α 2,6 sialic acid, with CS01-A4 and CS01-A7 exhibiting a higher binding affinity compared to CS01. As a control, the H1N1 human influenza virus bound effectively to α 2,6 sialic acid, whereas the H9N2 AIV did not exhibit binding to α 2,6 sialic acid. (d) presents the hemagglutination assay results using α 2,3 RBCs, which show that all three H4N1 AIVs and H9N2 AIV are capable of binding to α 2,3 sialic acid. The H1N1 human influenza virus did not exhibit binding to α 2,3 sialic acid

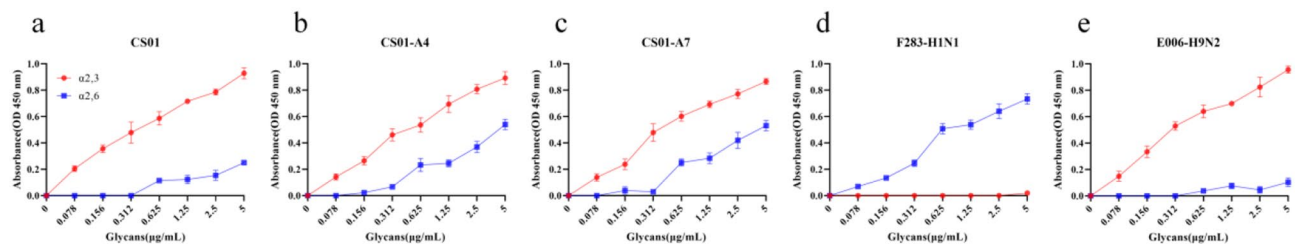


Fig. 3 The results of the solid-phase binding assay for H4N1 AIVs. The assay quantified the viruses' direct binding capacity to sialylated glycopolymers that contained either α 2,3 sialic acid (depicted in red) or α 2,6 sialic acid (depicted in blue). Each data point represents the mean of three independent replicate experiments. (a-c) showed that CS01, CS01-A4, and CS01-A7 demonstrated the capability to bind to α 2,3 sialic acids. Additionally, all three viruses were capable of binding to α 2,6 sialic acids, and compared to CS01-A4 and CS01-A7, the binding affinity of CS01 is relatively weak. As a control, the human influenza virus F283-H1N1 binds exclusively to α 2,6 sialic acids (d), while the AIV E006-H9N2 primarily binds α 2,3 sialic acids (e)

that CS01-A4 and CS01-A7 exhibit a higher affinity for human receptors than CS01 does.

Host tissue tropism of H4N1

To further investigate the pathogenicity of the H4N1 AIV in humans, we tested its tissue tropism for the human respiratory tract. We performed fluorescence staining on paraffin-embedded sections of human lung and tracheal

tissues, using the virus strains CS01, CS01-A4, and CS01-A7. The findings revealed that all three H4N1 AIVs were capable of binding to both human tracheal and lung tissues (Fig. 4). These results further indicated that H4N1 AIVs can bind to human receptors and effectively adsorb onto human respiratory tract tissues.

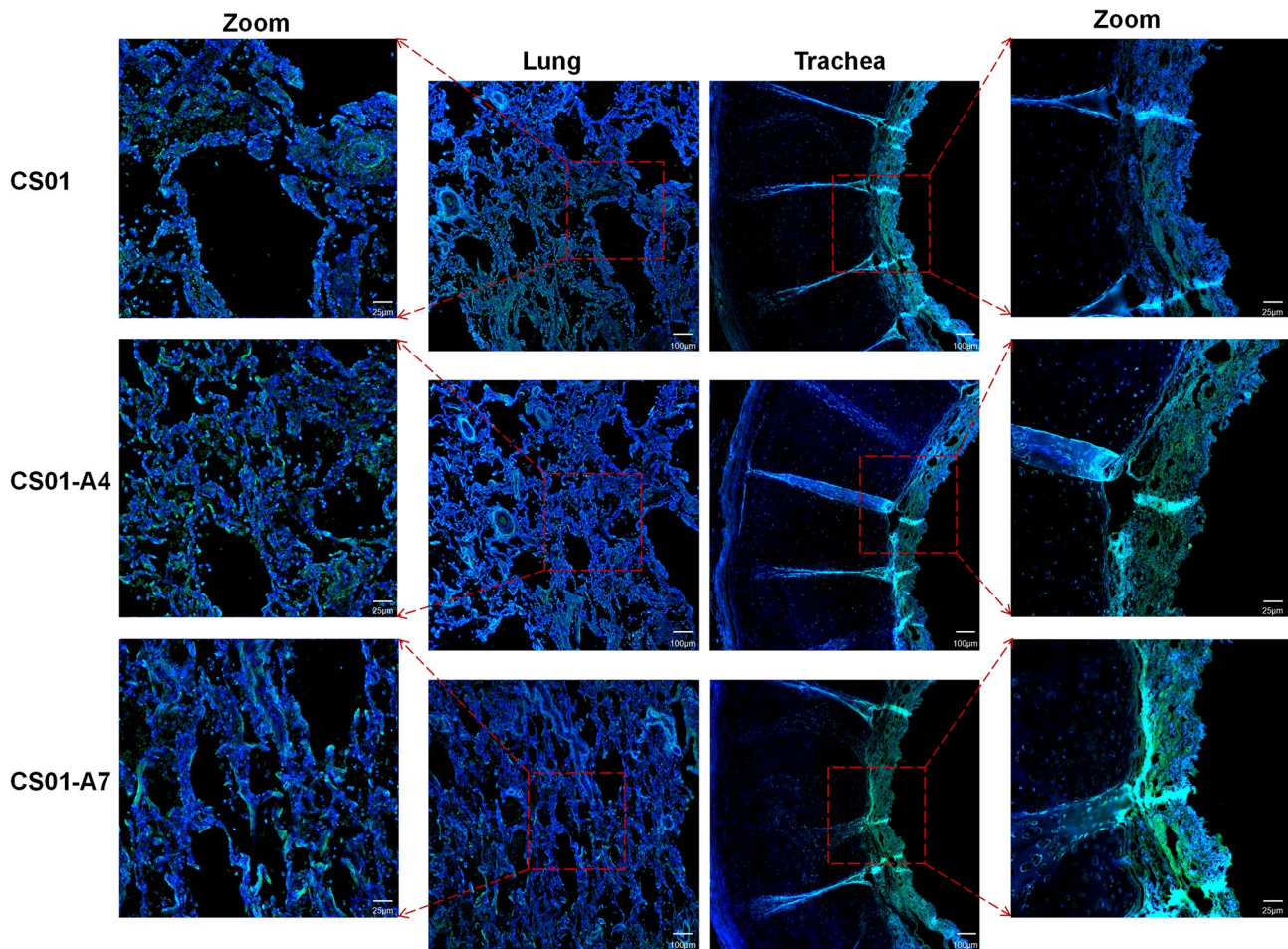


Fig. 4 Fluorescence staining of human lung and tracheal tissues infected with H4N1 AIVs. The image showed the binding of CS01, CS01-A4, and CS01-A7 to paraffin-embedded sections of human lung and tracheal tissues. Green fluorescence indicated virus binding, and blue fluorescence marked the nucleus. The left image showed the staining of human lung tissue, with local enlargements for CS01, CS01-A4, and CS01-A7 revealing that the bronchiolar and alveolar area of lungs were stained green. The right image displays the staining of tracheal tissue, with local enlargements showing that the tracheal mucosal layer and submucosal layer were stained green. This experiment was replicated three times, and representative images are shown. The images were taken by a fluorescence microscope (Olympus)

Growth kinetics of H4N1 in MDCK cells

The proteolytic activation of the influenza virus HA by cellular enzymes is indispensable for the virus to transform into an infectious form [25]. Pathogenicity of AIVs correlates directly with the ability of the viruses to produce cleaved HA in infected cells in culture [26]. HA could be cleaved by the addition of enzymes such as trypsin or plasmin to the growth medium and that this resulted in the enhancement of plaque-forming ability and a significant increase in virus yields [27]. To assess the dependence of H4N1 AIV replication on exogenous proteases, we inoculated minimal amounts of the CS01, CS01-A4, and CS01-A7 virus strains into MDCK cells and supplemented the serum-free medium with varying concentrations of exogenous proteases (2, 1, and 0 µg/mL of trypsin treated with N-p-tosyl-L-phenylalanine chloromethyl ketone (TPCK)). The virus growth kinetics and cytopathic effects (CPE) were monitored for a

period of 72 h post-inoculation. To assess the replication of the virus, we used the copy number of the M gene as a metric, in lieu of the traditionally employed TCID₅₀ or plaque-forming units (PFU). This decision was made because TCID₅₀ and PFU are less sensitive to detecting very low virus titers, which could result in misleading negative outcomes. Results indicate that at a concentration of 2 µg/mL TPCK-trypsin, CS01, CS01-A4, and CS01-A7 replicated efficiently, with viral loads peaking at 36 h post-inoculation (hpi), after which they declined gradually. Among these, CS01-A7 exhibited the highest viral load at the peak. Prior to reaching peak replication, the replication efficiency of CS01-A7 was significantly greater than that of CS01 and CS01-A4 ($P < 0.05$; see Supplementary Table S1), and its cytopathic effect (CPE) manifested earlier as well. When the concentration of TPCK-trypsin was reduced to 1 µg/mL, all three strains remained capable of effective replication, although

differences in replication efficiency began to emerge. Apart from no significant difference observed at 12 hpi, the replication efficiency of CS01-A7 was the highest ($P < 0.05$ for all other time points). In the absence of added TPCK-trypsin, none of the three strains was able to replicate. These findings revealed that all three H4N1 AIV strains required the addition of exogenous proteases to replicate efficiently in MDCK cells, suggesting that they possess low pathogenicity. Additionally, the replication capacity of CS01-A7 in MDCK cells was superior to that of the other two strains (Fig. 5).

Growth kinetics of H4N1 in human cells and avian cells

Testing the replication ability of pathogenicity-associated mutant viruses in different host cells is a common method for emulating host-switching events in vitro [28]. To assess the zoonotic potential of H4N1 AIVs in humans and poultry, we inoculated CS01, CS01-A4, and CS01-A7 into A549 and DF-1, and monitored virus growth kinetics up to 72 hpi. This method was designed to simulate the replication of H4N1 AIVs in humans and chickens in vitro. The results (Fig. 6) indicated that all three virus strains replicated efficiently in both A549 and DF-1

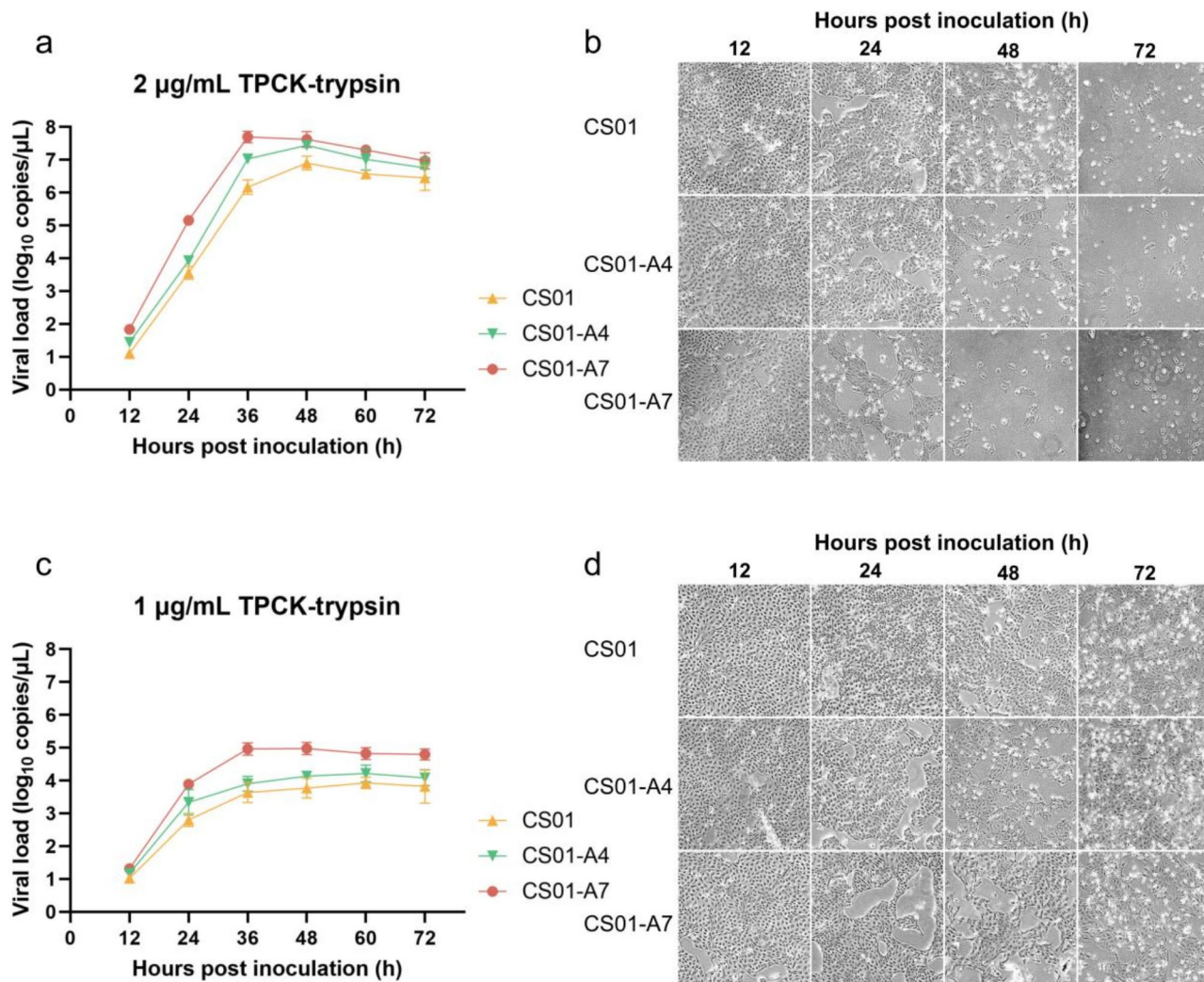


Fig. 5 Replication kinetics of H4N1 AIVs in MDCK cells across different concentrations of TPCK-trypsin (a, c). MDCK cells were inoculated in triplicate with a multiplicity of infection (MOI) of 0.0001. Post-inoculation, the cells were incubated at 37 °C, and culture supernatants were collected at 12, 24, 36, 48, 60, and 72 h post-inoculation (hpi) for viral load measurement using digital PCR (dPCR). Cytopathic effects (CPE) were monitored using an inverted phase contrast microscope (Olympus) at ×100 magnification (b, d). (a) The growth curve indicates that at a TPCK-trypsin concentration of 2 μg/mL, the average viral load of CS01, CS01-A4, and CS01-A7 rapidly increased until 36 hpi, followed by a gradual decline. Notably, the viral load of CS01-A7 was significantly higher than that of CS01 and CS01-A4 prior to 36 hpi. (b) By 24 hpi, pronounced CPE was observed in CS01-A7; however, significant CPE in CS01 and CS01-A4 was evident at 48 hpi. (c) At a TPCK-trypsin concentration of 1 μg/mL, the growth curve shows that the average viral loads of CS01, CS01-A4, and CS01-A7 increased over time, except at 72 hpi. Moreover, except for 12 hpi, the viral load of CS01-A7 remained higher than that of the other viruses. Each data point represents the mean of three independent replicate experiments, and the CPE images are representative selections. Statistical significance between viral loads at each hpi was analyzed by two-way analysis of variance (ANOVA) with Tukey’s multiple comparisons test (Supplementary Table S1)

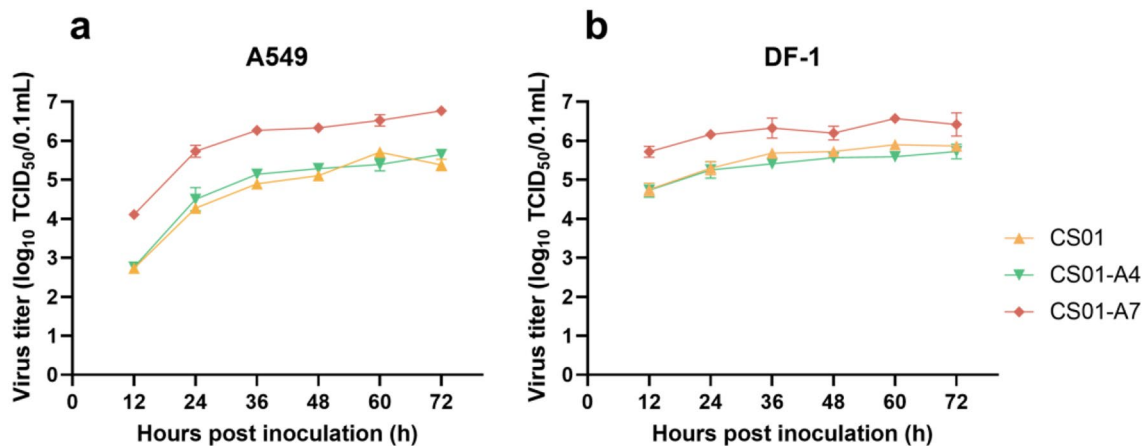


Fig. 6 Replication kinetics of H4N1 AIVs in A549 (a) and DF-1 (b) cells. A549, DF-1 were inoculated in triplicate with an MOI of 0.01. Post-inoculation, the cells were incubated at 37 °C, and culture supernatants were collected at 12, 24, 36, 48, 60, and 72 hpi for viral titer measurement. Viral titers were determined by titration in MDCK cells and expressed as TCID₅₀. Each data point represents the mean of three independent replicate experiments. Statistical significance between viral load at each hpi was analyzed by two-way analysis of variance (ANOVA) with Tukey's multiple comparisons test (Supplementary Table S2)

cells. Furthermore, regardless of the cell type, CS01-A7 exhibited a higher replication efficiency than the other two strains, a difference that was statistically significant ($p < 0.05$). These results further suggest that H4N1 AIVs can pose a threat to humans. Meanwhile, the replication ability of CS01-A7 is stronger than that of the other two viruses.

Pathogenicity and replication of the H4N1 AIVs in mice

Mice have been an animal model for studying influenza [29]. Figure 7a showed the pattern of body weight loss in the inoculated mice: all three H4N1 AIVs induced a decrease in body weight compared to the PBS control. Notably, mice inoculated with CS01-A7 exhibited a more pronounced loss of body weight than those inoculated with the other two virus strains. Figure 7b displayed the virus titers in tissue samples: high titers were detected in the lungs, tracheas, and nasal turbinates at 3 and 6 days post-inoculation (dpi). Specifically, at 3 dpi, the titers of CS01-A7 in these respiratory organs were significantly higher than those of the other two strains ($P < 0.05$). Furthermore, no virus was detected in the kidneys or brain tissues (limit of detection was 100 TCID₅₀/0.1 g). These findings suggest that all three H4N1 AIVs could decrease mouse body weight without prior adaptation and effectively replicate within the murine respiratory tract. However, none of the viruses caused mouse mortality or replicated efficiently in the urinary or nervous systems, indicating their low pathogenicity. Importantly, CS01-A7 demonstrated a greater ability to induce body weight loss and replicate in the respiratory tract compared to the other two viruses.

Histopathological analysis of the H4N1 AIVs in mice

To further assess the pathogenic effects of H4N1 avian influenza viruses on mice, we conducted paraffin embedding and sectioning of lung and tracheal tissues from virus-inoculated mice. Hematoxylin-eosin (HE) staining was then performed to visualize and characterize the pathological alterations within these tissue samples. Figure 8a-c illustrates the HE staining results of lung tissue sections, revealing that all three H4N1 AIVs induced lung lesions, with varying degrees of severity. Similarly, as shown in Fig. 8d-f, tracheal sections displayed lesions, including ciliary necrosis and detachment, across all samples. In summary, all H4N1 AIVs induced pathological changes in the respiratory tract, with the CS01-A7 virus strain causing more pronounced lesions compared to the other two strains.

Discussion

In this study, we demonstrated that H4N1 AIV has the capacity to bind to human receptors, effectively adsorb onto human respiratory tract tissues, and replicate efficiently in human lung cells. These findings suggest its potential for cross-species transmission to humans, which is consistent with the hypotheses proposed by previous bioinformatics predictions [30]. Furthermore, H4N1 AIV induced symptoms of pneumonia and tracheitis in mice without the need for prior adaptation, highlighting their mammalian pathogenicity. Additionally, during a limited number of in vitro cell passages (4 and 7 passages), novel mutations arose in the HA and NP of H4N1 AIV. These mutations enhanced the virus's binding affinity to human-type $\alpha 2,6$ -linked sialic acid receptors, accelerated replication kinetics in mammalian cells, and increased murine pathogenicity. These traits—receptor

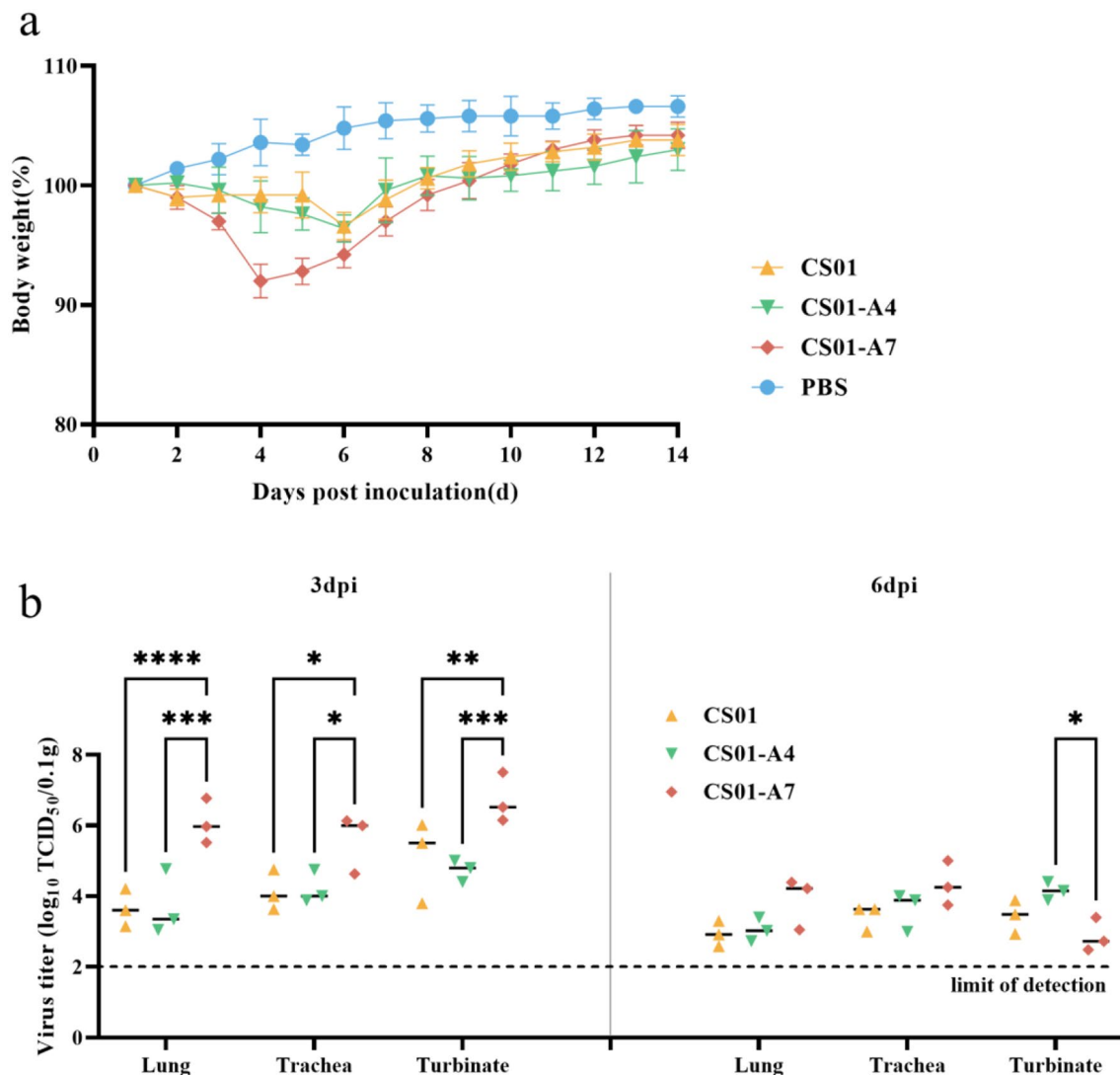


Fig. 7 Pathogenicity and replication capacity of H4N1 avian influenza viruses in BALB/c mice. **(a)** Body weight change kinetics in mice inoculated with CS01, CS01-A4, CS01-A7, and PBS (control). **(b)** Virus titers in various mouse organs at 3 and 6 dpi. Tissue samples were weighed, and virus titers were determined by titration in MDCK cells, with results reported as TCID₅₀ per 0.1 g of tissue. Data points represent the mean of three independent experiments. Statistical significance is denoted by the number of asterisks, with * indicating $P < 0.05$, ** $P < 0.01$, *** $P < 0.001$, and **** $P < 0.0001$

adaptation, enhanced replication efficiency, and heightened mammalian virulence—demonstrate H4N1 AIV's capacity to rapidly evolve phenotypes conducive to cross-species infection under controlled laboratory conditions. While this does not equate to proven zoonotic transmission, it highlights the risks and emphasizes the necessity of actively monitoring H4N1 AIV.

The receptor-binding preference of HA is crucial for influenza virus replication and transmission; binding to $\alpha 2,6$ sialic acids is a prerequisite for an influenza virus to transmit efficiently among humans [31]. We found that H4N1 AIV can effectively bind to $\alpha 2,6$ sialic acid and recognize human receptors. Notably, the R467Q mutation in the HA protein enhances the virus's ability to bind to human receptors. Although it is generally believed that

alterations in the virus's receptor-binding ability are primarily caused by variations near the HA pocket structure (the 130-loop, 190-helix, and 220-loop) [32], both our hemagglutination assay and solid-phase binding assay confirmed that the R467Q mutation enhances the binding of H4N1 AIV to human receptors. This finding indicates that changes distant from the pocket structure can also impact the virus's receptor-binding ability.

NP is well-established as a key player in the influenza virus life cycle, with essential roles in both transcription and replication of the viral RNA segments [33, 34]. Our study found that the A428T mutation in the NP of H4N1 AIV significantly enhanced the virus's replication ability. Experimental data revealed that mice infected with the A428T mutant strain (CS01-A7) exhibited higher

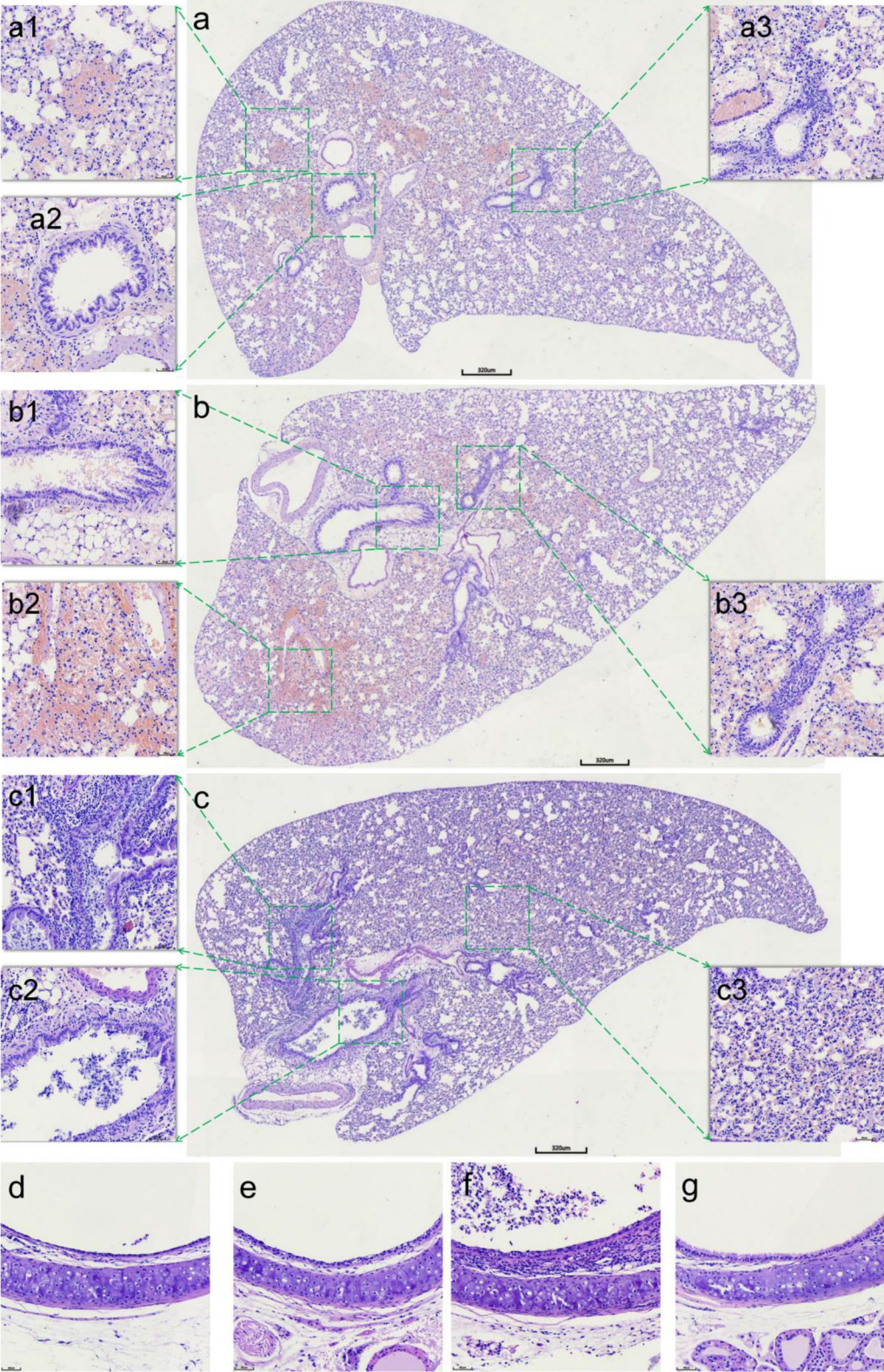


Fig. 8 (See legend on next page.)

(See figure on previous page.)

Fig. 8 Histopathological examination of lung and tracheal tissues from mice inoculated with H4N1 AIVs. **(a)** HE-stained lung sections at 3 dpi with CS01, showing slight hemorrhage (a1), epithelial cell shedding (a2), and lymphocyte aggregation (a3). **(b)** Lung sections from mice inoculated with CS01-A4 at 3 dpi, revealing bronchial epithelial cell shedding (b1), pulmonary hemorrhage (b2), and lymphocyte aggregation (b3). **(c)** Lung sections from mice inoculated with CS01-A7 at 3 dpi, demonstrating lung consolidation, extensive lymphocyte infiltration around the trachea (c1), necrosis and shedding of bronchial epithelial cells (c2), inflammatory cell infiltrates in alveolar cavities, and intra-alveolar hemorrhage (c3). **(d-f)** HE-stained tracheal sections at 3 dpi with CS01, CS01-A4, and CS01-A7, respectively, showing ciliary necrosis and shedding in **(d)** and **(e)**, and more severe changes including necrosis, shedding of epithelial tissue, tracheal wall thickening, and lymphocyte infiltration in **(f)**. **(g)** HE-stained tracheal section from the control group, showing normal tissue structure. Images were acquired using a digital slide scanning system (Zeiss). In the inserts surrounding figures a, b, and c, the images were magnified tenfold

virus titers in respiratory tract tissues compared to those infected with the wild-type virus (lacking the A428T mutation). This enhanced replication ability was also confirmed in vitro, where the A428T mutation led to a significant increase in the efficiency of virus replication in A549 and MDCK cell cultures. We speculate that the A428T mutation may alter the NP protein's interaction with the viral RNA polymerase complex or the RNA segments themselves, thereby improving the efficiency of viral RNA synthesis and enhancing the virus's replication ability in both cell culture and in vivo. Furthermore, the increased replication in the respiratory tract led to the heightened pathogenicity observed in mice, as it allows for more extensive damage to the lung tissue and a more robust immune response.

Additionally, our observations revealed that the H4N1 AIV is unable to replicate efficiently in MDCK cells without exogenous proteases and does not result in mortality in experimental mice, indicative of its low pathogenic profile. Nevertheless, research has indicated that the H4 subtype AIV has the potential to mutate into a highly pathogenic phenotype [35]. Given the increasing prevalence in mammalian hosts globally and the notable annual rise in isolation frequency [10, 36], coupled with the capability for rapid mutation of H4N1 AIV observed in this study, H4 subtype AIVs may be evolving into a highly pathogenic form. This necessitates vigilance and further surveillance.

AIV is a globally prevalent pathogen that persists and spreads among various wild and domestic animal species. This virus is known for its capacity to undergo frequent gene rearrangements and mutations, which enables it to adapt to new hosts and environments quickly. In line with the “One Health” principle—which posits that environmental, animal, and human health are inextricably linked—it is essential to acknowledge the potential threat that AIV poses to human health. Furthermore, the “streetlight effect” mentioned in the World Health Organization's Disease X Report highlights the need to enhance the monitoring of potential diseases beyond those that are most visible or currently understood [37]. Therefore, it is very important to carry out strict and continuous monitoring of various AIVs and to disseminate the research results in a timely manner. Measures such as expanding monitoring of wild birds, strengthening

monitoring of poultry, conducting AIV screening for patients with severe respiratory diseases, actively developing epidemic response plans, enhance public awareness and international coordination are not only beneficial but also crucial for reducing the public health risks posed by AIVs.

Our study has several limitations. The in vivo experiments were performed in a limited number of mice, which may not fully represent the potential pathogenicity of H4N1 AIVs. Additionally, the experiments focused on mice, which may not fully recapitulate the disease progression observed in other mammals. Additional studies in other mammalian models, such as ferrets or guinea pig, would provide a more comprehensive understanding of H4N1 AIV pathogenesis. Finally, our study offers preliminary experimental evidence for the emerging zoonotic potential of H4N1 AIV, and further research is still needed to investigate environmental fitness, immune evasion, and transmissibility.

In summary, our research on H4N1 AIV is the first to elucidate its pathogenic potential in humans, highlight the risk of the H4 subtype transitioning into a zoonotic pathogen, and underscore the importance of continued monitoring of AIVs.

Abbreviations

IAV	Influenza A virus
AIV	Avian influenza virus
HA	Hemagglutinin
NA	Neuraminidase
CPE	Cytopathic effect
GISAID	Global Initiative on Sharing All Influenza Data
MDCK	Madin-Darby Canine Kidney
A549	Human type II alveolar epithelial
DF-1	Chicken-origin fibroblast
TCID ₅₀	The 50% tissue culture infectious dose
ORFs	Open reading frames
MOI	Multiplicity of infections
dpi	Days post-inoculation
hpi	Hours post-inoculation

Supplementary Information

The online version contains supplementary material available at <https://doi.org/10.1186/s12985-025-02736-4>.

Supplementary Material 1

Supplementary Material 2

Supplementary Material 3

Acknowledgements

We express our sincere appreciation to all contributors who have uploaded data to the GISAID database. We are especially grateful to Professor Ling Hua, Chief Scientist at the Chongqing Center for Disease Control and Prevention, for her essential contributions to this study. Additionally, we thank Ms. Yu Fengqin and Ms. Jing Song for their insightful suggestions, which have significantly enhanced our research.

Author contributions

XP, XW and JD contributed equally to this work and should be considered co-first authors. XP, XW, JD and SC conceived and designed the assays. XP, XW, JD, MY, YL, YZ, XB, GJ, XL, FY, PL, YT, ZT, ZY and SY conducted experimental work. XP, XW and JD analysed the data and wrote the paper. All authors read and approved the final manuscript.

Funding

This work was funded by the Changshou Science Foundation (Grant Number CSKJ2024059).

Data availability

All virus sequences generated during this study have been deposited in the GISAID database, Isolate ID: EPI_ISL_18455199, EPI_ISL_19319390, EPI_ISL_19319391.

Declarations

Ethics approval and consent to participate

Animal experiments were approved by the Institutional Animal Care and Use Committee (IACUC) of Charles River Laboratories (Permission number: BJ-GE-24-139), and all procedures complied with the welfare standards for laboratory animals.

Consent for publication

The authors agree to publication.

Competing interests

The authors declare no competing interests.

Received: 23 January 2025 / Accepted: 10 April 2025

Published online: 18 April 2025

References

- Cox NJ, Subbarao K. Global epidemiology of influenza: past and present. *Annu Rev Med*. 2000;51:407–21. <https://doi.org/10.1146/annurev.med.51.1.407>.
- Webster RG, Bean WJ, Gorman OT, Chambers TM, Kawaoka Y. Evolution and ecology of influenza A viruses. *Microbiol Rev*. 1992;56(1):152–79. <https://doi.org/10.1128/mr.56.1.152-179.1992>.
- Olsen B, Munster VJ, Wallensten A, Waldenström J, Osterhaus AD, Fouchier RA. Global patterns of influenza A virus in wild birds. *Science*. 2006;312(5772):384–8. <https://doi.org/10.1126/science.1122438>.
- Wu Y, Wu Y, Tefsen B, Shi Y, Gao GF. Bat-derived influenza-like viruses H17N10 and H18N11. *Trends Microbiol*. 2014;22(4):183–91. <https://doi.org/10.1016/j.tim.2014.01.010>.
- Yoon SW, Webby RJ, Webster RG. Evolution and ecology of influenza A viruses. *Curr Top Microbiol Immunol*. 2014;385:359–75. https://doi.org/10.1007/782_2014_396.
- Wang D, Zhu W, Yang L, Shu Y. The epidemiology, virology, and pathogenicity of human infections with avian influenza viruses. *Cold Spring Harb Perspect Med*. 2021;11(4):a038620. <https://doi.org/10.1101/cshperspect.a038620>.
- http://www.who.int/influenza/human_animal_interface/
- Uyeki TM, Milton S, Abdul Hamid C, Reinoso Webb C, Presley SM, Shetty V, Rollo SN, Martinez DL, Rai S, Gonzales ER, Kniss KL, Jang Y, Frederick JC, De La Cruz JA, Liddell J, Di H, Kirby MK, Barnes JR, Davis CT. Highly pathogenic avian influenza A(H5N1) virus infection in a dairy farm worker. *N Engl J Med*. 2024;390(21):2028–9. <https://doi.org/10.1056/NEJMc2405371>.
- Wille M, Tolf C, Latorre-Margalef N, Fouchier RAM, Halpin RA, Wentworth DE, Ragwani J, Pybus OG, Olsen B, Waldenström J. Evolutionary features of a prolific subtype of avian influenza A virus in European waterfowl. *Virus Evol*. 2022;8(2):veac074. <https://doi.org/10.1093/ve/veac074>.
- Bo H, Zhang Y, Dong J, Li XY, Liu J, Tan M, Zhao X, Wang DY. [Distribution and gene characteristics of H3, H4 and H6 subtypes of low pathogenic avian influenza viruses in environment related avian influenza viruses during 2014–2021 in China]. *Zhonghua Yu Fang Yi Xue Za Zhi*. 2022;56(11):1549–53. <https://doi.org/10.3760/cmaj.cn112150-20220810-00803>. Chinese.
- Henriques AM, Fagulha T, Barros SC, Ramos F, Duarte M, Luís T, Fevereiro M. Multiyear surveillance of influenza A virus in wild birds in Portugal. *Avian Pathol*. 2011;40(6):597–602. <https://doi.org/10.1080/03079457.2011.618943>.
- Toennessen R, Germundsson A, Jonassen CM, Haugen I, Berg K, Barrett RT, Rimstad E. Virological and serological surveillance for type A influenza in the black-legged Kittiwake (*Rissa tridactyla*). *Virology*. 2011;8:21. <https://doi.org/10.186/1743-422X-8-21>.
- Wu H, Peng X, Cheng L, Lu X, Jin C, Xie T, Yao H, Wu N. Genetic characterization of natural reassortant H4 subtype avian influenza viruses isolated from domestic ducks in Zhejiang Province in China from 2013 to 2014. *Virus Genes*. 2015;51(3):347–55. <https://doi.org/10.1007/s11262-015-1245-2>.
- Okamoto M, Nishi T, Nomura N, Yamamoto N, Sakoda Y, Sakurai K, Chu HD, Thanh LP, Van Nguyen L, Van Hoang N, Tien TN, Yoshida R, Takada A, Kida H. The genetic and antigenic diversity of avian influenza viruses isolated from domestic ducks, muscovy ducks, and chickens in Northern and Southern Vietnam, 2010–2012. *Virus Genes*. 2013;47(2):317–29. <https://doi.org/10.1007/s11262-013-0954-7>.
- Hinshaw VS, Bean WJ, Webster RG, Rehg JE, Fiorelli P, Early G, Geraci JR, St Aubin DJ. Are seals frequently infected with avian influenza viruses? *J Virol*. 1984;51(3):863–5. <https://doi.org/10.1128/JVI.51.3.863-865.1984>.
- Hu Y, Liu X, Li S, Guo X, Yang Y, Jin M. Complete genome sequence of a novel H4N1 influenza virus isolated from a pig in central China. *J Virol*. 2012;86(24):13879. <https://doi.org/10.1128/JVI.02726-12>.
- Xu Y, Tang L, Gu X, Bo S, Ming L, Ma M, Zhao C, Sun K, Liu Y, He G. Characterization of avian influenza A (H4N2) viruses isolated from wild birds in Shanghai during 2019 to 2021. *Poult Sci*. 2023;102(10):102948. <https://doi.org/10.1016/j.psj.2023.102948>.
- Reid SM, Brookes SM, Núñez A, Banks J, Parker CD, Ceeraz V, Russell C, Seekings A, Thomas SS, Puranik A, Brown IH. Detection of non-notifiable H4N6 avian influenza virus in poultry in great Britain. *Vet Microbiol*. 2018;224:107–15. <https://doi.org/10.1016/j.vetmic.2018.08.026>.
- Shibuya N, Goldstein IJ, Broekaert WF, Nsimba-Lubaki M, Peeters B, Peumans WJ. The Elderberry (*Sambucus nigra* L.) bark lectin recognizes the Neu5Ac(alpha 2-6)Gal/GalNAc sequence. *J Biol Chem*. 1987;262(4):1596–601.
- Wang WC, Cummings RD. The immobilized leucoagglutinin from the seeds of *Maackia amurensis* binds with high affinity to complex-type Asn-linked oligosaccharides containing terminal Sialic acid-linked alpha-2,3 to penultimate galactose residues. *J Biol Chem*. 1988;263(10):4576–85.
- Sun Y, Qin K, Wang J, Pu J, Tang Q, Hu Y, Bi Y, Zhao X, Yang H, Shu Y, Liu J. High genetic compatibility and increased pathogenicity of reassortants derived from avian H9N2 and pandemic H1N1/2009 influenza viruses. *Proc Natl Acad Sci U S A*. 2011;108(10):4164–9. <https://doi.org/10.1073/pnas.1019109108>.
- Liu K, Ding P, Pei Y, Gao R, Han W, Zheng H, Ji Z, Cai M, Gu J, Li X, Gu M, Hu J, Liu X, Hu S, Zhang P, Wang X, Wang X, Liu X. Emergence of a novel reassortant avian influenza virus (H10N3) in Eastern China with high pathogenicity and respiratory droplet transmissibility to mammals. *Sci China Life Sci*. 2022;65(5):1024–35. <https://doi.org/10.1007/s11427-020-1981-5>.
- Long JS, Mistry B, Haslam SM, Barclay WS. Host and viral determinants of influenza A virus species specificity. *Nat Rev Microbiol*. 2019;17(2):67–81. <https://doi.org/10.1038/s41579-018-0115-z>. Erratum in: *Nat Rev Microbiol*. 2019;17(2):124. doi: 10.1038/s41579-018-0140-y.
- Paulson JC, Rogers GN. Resialylated erythrocytes for assessment of the specificity of sialyloligosaccharide binding proteins. *Methods Enzymol*. 1987;138:162–8. [https://doi.org/10.1016/0076-6879\(87\)38013-9](https://doi.org/10.1016/0076-6879(87)38013-9).
- Steinhauer DA. Role of hemagglutinin cleavage for the pathogenicity of influenza virus. *Virology*. 1999;258(1):1–20. <https://doi.org/10.1006/viro.1999.716>.
- Bosch FX, Orlich M, Klenk HD, Rott R. The structure of the hemagglutinin, a determinant for the pathogenicity of influenza viruses. *Virology*. 1979;95(1):197–207. [https://doi.org/10.1016/0042-6822\(79\)90414-8](https://doi.org/10.1016/0042-6822(79)90414-8).
- Appleyard G, Maber HB. Plaque formation by influenza viruses in the presence of trypsin. *J Gen Virol*. 1974;25(3):351–7. <https://doi.org/10.1099/0022-1317-25-3-351>.
- Liu K, Guo Y, Zheng H, Ji Z, Cai M, Gao R, Zhang P, Liu X, Xu X, Wang X, Liu X. Enhanced pathogenicity and transmissibility of H9N2 avian influenza virus in

- mammals by hemagglutinin mutations combined with PB2-627K. *Virology*. 2023;38(1):47–55. <https://doi.org/10.1016/j.virus.2022.09.006>.
29. HARFORD CG. Effect of influenza virus on cilia and epithelial cells in the bronchi of mice. *J Exp Med*. 1952;95(2):173–90. <https://doi.org/10.1084/jem.95.2.173>.
 30. He J, Deng J, Wen X, Yan M, Liu Y, Zhou Y, Du X, Yang H, Peng X. Isolation and genetic characteristics of novel H4N1 avian influenza viruses in ChongQing, China. *Virology*. 2024;21(1):85. <https://doi.org/10.1186/s12985-024-02352-8>.
 31. Zhang Y, Zhang Q, Gao Y, He X, Kong H, Jiang Y, Guan Y, Xia X, Shu Y, Kawaoka Y, Bu Z, Chen H. Key molecular factors in hemagglutinin and PB2 contribute to efficient transmission of the 2009 H1N1 pandemic influenza virus. *J Virol*. 2012;86(18):9666–74. <https://doi.org/10.1128/JVI.00958-12>.
 32. Shi Y, Wu Y, Zhang W, Qi J, Gao GF. Enabling the 'host jump': structural determinants of receptor-binding specificity in influenza A viruses. *Nat Rev Microbiol*. 2014;12(12):822–31. <https://doi.org/10.1038/nrmicro3362>.
 33. Honda A, Uéda K, Nagata K, Ishihama A. RNA polymerase of influenza virus: role of NP in RNA chain elongation. *J Biochem*. 1988;104(6):1021–6. <https://doi.org/10.1093/oxfordjournals.jbchem.a122569>.
 34. Biswas SK, Boutz PL, Nayak DP. Influenza virus nucleoprotein interacts with influenza virus polymerase proteins. *J Virol*. 1998;72(7):5493–501. <https://doi.org/10.1128/JVI.72.7.5493-5501.1998>.
 35. Veits J, Weber S, Stech O, Breithaupt A, Gräber M, Gohrbandt S, Bogs J, Hundt J, Teifke JP, Mettenleiter TC, Stech J. Avian influenza virus hemagglutinins H2, H4, H8, and H14 support a highly pathogenic phenotype. *Proc Natl Acad Sci U S A*. 2012;109(7):2579–84. <https://doi.org/10.1073/pnas.1109397109>. Epub 2012 Jan 30.
 36. Luo S, Xie Z, Xie L, Huang L, Huang J, Deng X, Zeng T, Wang S, Zhang Y, Liu J. Surveillance of live poultry markets for low pathogenic avian influenza viruses in Guangxi Province, Southern China, from 2012–2015. *Sci Rep*. 2017;7(1):17577. <https://doi.org/10.1038/s41598-017-17740-0>.
 37. <https://www.who.int/news/item/01-08-2024-cepi-and-who-urge-broader-research-strategy-for-countries-to-prepare-for-the-next-pandemic>

Publisher's note

Springer Nature remains neutral with regard to jurisdictional claims in published maps and institutional affiliations.